Article

Molecular Cell

KDM3A Senses Oxygen Availability to Regulate PGC-1α-Mediated Mitochondrial Biogenesis

Graphical Abstract

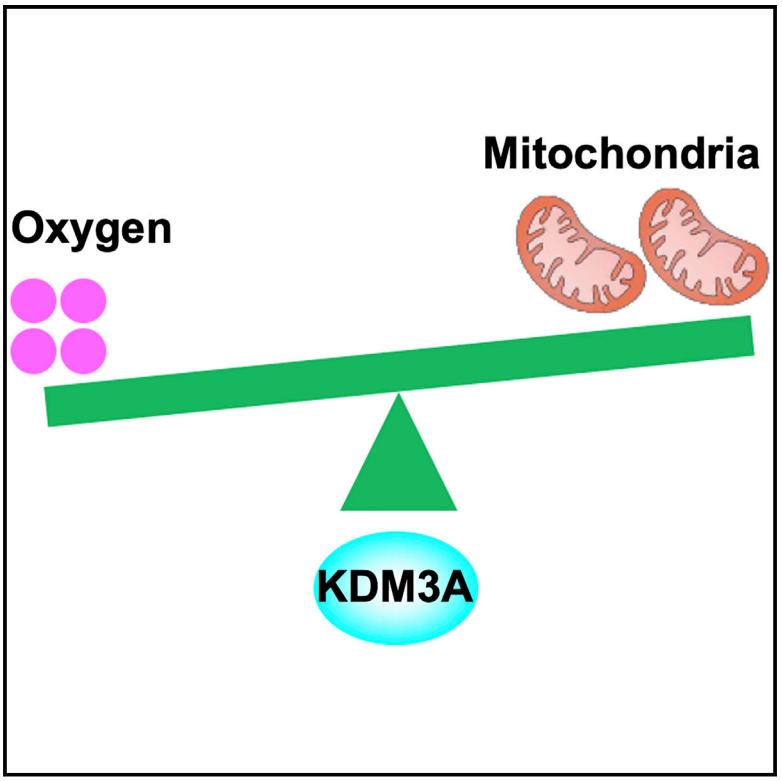

Authors

Xu Qian, Xinjian Li, Zhumei Shi, ..., Zhibin Hu, Qin Zhou, Zhimin Lu

Correspondence

xqianmedres@njmu.edu.cn (X.Q.), zhiminlu@zju.edu.cn (Z.L.)

In Brief

Qian et al. demonstrated that KDM3A functions as an oxygen sensor and demethylates K224-monomethylated PGC-1α under normoxic conditions. Hypoxia inhibits KDM3A activity and increases PGC-1α K224 monomethylation, resulting in the inhibition of PGC-1α and PGC-1α-dependent mitochondrial biogenesis, a decrease of ROS levels and apoptosis, and the promotion of brain tumor development.

Highlights

- Hypoxia suppresses mitochondrial biogenesis of tumor cells
- PGC-1α's activity is inhibited by K224 monomethylation under hypoxic conditions
- KDM3A senses oxygen availability for its activity and demethylates PGC-1α
- PGC-1α monomethylation reduces hypoxia-induced ROS and apoptosis for tumor growth

Qian et al., 2019, Molecular Cell *76*, 1–11
December 19, 2019
https://doi.org/10.1016/j.molcel.2019.09.019

CellPress

Please cite this article in press as: Qian et al., KDM3A Senses Oxygen Availability to Regulate PGC-1α-Mediated Mitochondrial Biogenesis, Molecular Cell (2019), https://doi.org/10.1016/j.molcel.2019.09.019

Molecular Cell
Article

KDM3A Senses Oxygen Availability to Regulate PGC-1α-Mediated Mitochondrial Biogenesis

Xu Qian,[1,2,13,*] Xinjian Li,[3,13] Zhumei Shi,[4] Xiaoming Bai,[5] Yan Xia,[6] Yanhua Zheng,[6] Daqian Xu,[6] Feng Chen,[7] Yongping You,[4] Jing Fang,[8] Zhibin Hu,[9,10] Qin Zhou,[11] and Zhimin Lu[12,14,*]

[1]Department of Nutrition and Food Hygiene, Center for Global Health, School of Public Health, Nanjing Medical University, Nanjing, Jiangsu 211166, China
[2]Institute for Brain Tumors, Jiangsu Key Lab of Cancer Biomarkers, Prevention and Treatment, Jiangsu Collaborative Innovation Center for Cancer Personalized Medicine, Nanjing Medical University, Nanjing, Jiangsu 211166, China
[3]CAS Key Laboratory of Infection and Immunity, CAS Center for Excellence in Biomacromolecules, Institute of Biophysics, Chinese Academy of Sciences, Beijing 100101, China
[4]Department of Neurosurgery, The First Affiliated Hospital of Nanjing Medical University, Nanjing, Jiangsu 210029, China
[5]Department of Pathology, School of Basic Medical Sciences, Nanjing Medical University, Nanjing, Jiangsu 211166, China
[6]Brain Tumor Center and Department of Neuro-Oncology, The University of Texas MD Anderson Cancer Center, Houston, TX 77030, USA
[7]Department of Forensic Medicine, School of Basic Medical Sciences, Nanjing Medical University, Nanjing, Jiangsu 211166, China
[8]The Affiliated Hospital of Qingdao University, Qingdao Cancer Institute, Qingdao, Shandong 266061, China
[9]Department of Epidemiology, Center for Global Health, School of Public Health, Nanjing Medical University, Nanjing, Jiangsu 211166, China
[10]State Key Laboratory of Reproductive Medicine, China International Cooperation Center for Environment and Human Health, Nanjing Medical University, Nanjing, Jiangsu 211166, China
[11]The Ministry of Education Key Laboratory of Laboratory Medical Diagnostics, the College of Laboratory Medicine, Chongqing Medical University, Chongqing 400016, China
[12]Zhejiang Provincial Key Laboratory of Pancreatic Disease, The First Affiliated Hospital, and Institute of Translational Medicine, Zhejiang University School of Medicine, Hangzhou, Zhejiang 310029, China
[13]These authors contributed equally
[14]Lead Contact
*Correspondence: xqianmedres@njmu.edu.cn (X.Q.), zhiminlu@zju.edu.cn (Z.L.)
https://doi.org/10.1016/j.molcel.2019.09.019

SUMMARY

Hypoxia, which occurs during tumor growth, triggers complex adaptive responses in which peroxisome proliferator-activated receptor gamma coactivator-1 alpha (PGC-1α) plays a critical role in mitochondrial biogenesis and oxidative metabolism. However, how PGC-1α is regulated in response to oxygen availability remains unclear. We demonstrated that lysine demethylase 3A (KDM3A) binds to PGC-1α and demethylates monomethylated lysine (K) 224 of PGC-1α under normoxic conditions. Hypoxic stimulation inhibits KDM3A, which has a high K_M of oxygen for its activity, and enhances PGC-1α K224 monomethylation. This modification decreases PGC-1α's activity required for NRF1- and NRF2-dependent transcriptional regulation of *TFAM*, *TFB1M*, and *TFB2M*, resulting in reduced mitochondrial biogenesis. Expression of PGC-1α K224R mutant significantly increases mitochondrial biogenesis, reactive oxygen species (ROS) production, and tumor cell apoptosis under hypoxia and inhibits brain tumor growth in mice. This study revealed that PGC-1α monomethylation, which is dependent on oxygen availability-regulated KDM3A, plays a critical role in the regulation of mitochondrial biogenesis.

INTRODUCTION

Mitochondrial biogenesis is regulated by transcriptional programs that coordinate the induction of both mitochondria- and nucleus-localized genes that encode mitochondrial proteins (Vyas et al., 2016; Zong et al., 2016). The transcriptional coactivator peroxisome proliferator-activated receptor gamma coactivator-1α (PGC-1α) is a central regulator of certain nucleus-encoded mitochondrial genes through interactions with multiple transcription factors (Tan et al., 2016), including nuclear respiratory factor (NRF) 1 (Wu et al., 1999), NRF2 (also known as GABPA; Vercauteren et al., 2008), peroxisome proliferator-activated receptor α (PPARα) (Vega et al., 2000), estrogen-related receptor α (ERRα) (Huss et al., 2002), and yin-yang 1 (YY1) (Cunningham et al., 2007; Lin et al., 2005; Scarpulla et al., 2012).

NRF1 and NRF2, which are distinct from *NFE2L1* (nuclear factor, erythroid 2 like 1) and *NFE2L2* (nuclear factor, erythroid 2 like 2) genes responsible for ROS detoxification, although they share the same names in bibliographic databases, are able to stimulate the expression of mitochondrial transcription factor A (*TFAM*), mitochondrial transcription factor B1 (*TFB1M*), mitochondrial transcription factor B2 (*TFB2M*), and mitochondrial matrix proteins that are essential for the replication and transcription of mtDNA (Kelly and Scarpulla, 2004; Lin et al., 2005; Scarpulla et al., 2012; Wu et al., 1999). By activating these transcriptional factors, PGC-1α is capable of driving virtually all aspects of mitochondrial biogenesis, including the activation of respiratory chain and fatty acid oxidation enzyme genes, increase of mitochondrial

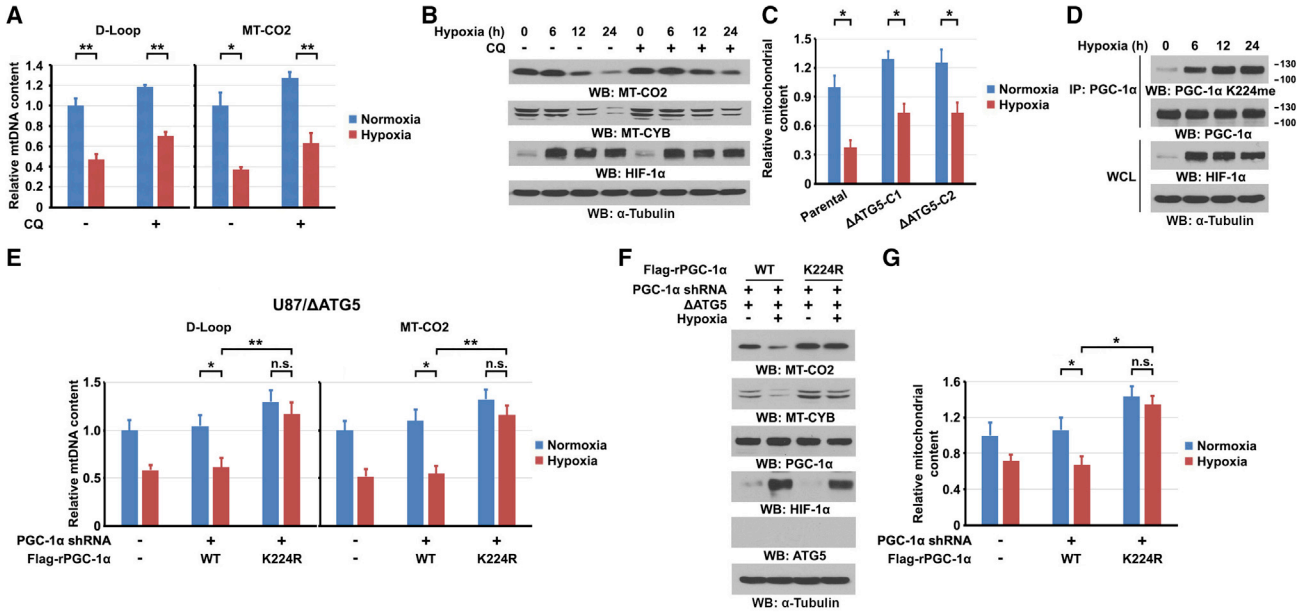

Figure 1. Hypoxia-Induced PGC-1α K224 Monomethylation Suppresses Mitochondrial Biogenesis

(A and B) U87 cells treated with or without 100 μM chloroquine diphosphate (CQ) were cultured with or without hypoxia for 24 h (A) or for the indicated periods of time (B). qPCR analyses (A) and immunoblotting analyses (B) were performed.

(C) Parental or ATG5-null (ΔATG5) U87 cells were treated with or without hypoxia for 24 h. qPCR analyses were performed. C1, clone 1; C2, clone 2.

(D) U87 cells were treated with hypoxia for the indicated periods of time. Immunoprecipitation and immunoblotting analyses were performed.

(E–G) ATG5-null U87 cells with or without depleted PGC-1α and reconstituted expression of shRNA-resistant (r) WT FLAG-rPGC-1α or FLAG-rPGC-1α K224R were cultured with or without hypoxia for 24 h. qPCR analyses (E), immunoblotting analyses (F), and fluorescence-activated cell sorting (FACS) analyses (G) were performed.

(A, C, E, and G) Data represent the mean ± SD from triplicate experiments. *$p < 0.05$; **$p < 0.001$; n.s., no significance. (B, D, and F) Immunoprecipitation and immunoblotting analyses were performed with the indicated antibodies. See also Figures S1 and S2.

numbers, and the augmentation of mitochondrial respiratory capacity (Kelly and Scarpulla, 2004; Lin et al., 2005; Scarpulla et al., 2012). PGC-1α has been reported to be responsible for a metabolic plasticity that likely supports drug resistance as well as metastasis (Andrzejewski et al., 2017; LeBleu et al., 2014; Luo et al., 2016; Torrano et al., 2016). Rapid tumor growth inevitably results in nutrient and oxygen stress, and hypoxia is a feature of solid tumor growth. Hypoxia has been shown to inhibit mitochondrial biogenesis through hypoxia-inducible factor 1α (HIF-1α)-dependent suppression of PGC-1β expression in Von Hippel-Lindau (VHL)-deficient renal cell carcinoma (Zhang et al., 2007). However, how PGC-1α-mediated mitochondrial biogenesis is regulated during oxygen stress is largely unclear.

In this study, we demonstrated that lysine demethylase 3A (KDM3A) functions as an oxygen sensor to demethylate monomethylated K224 of PGC-1α in an oxygen tension-dependent manner. Hypoxic stimulation inhibited KDM3A activity and enhanced the monomethylation of PGC-1α, which inhibited PGC-1α activity and thus reduced mitochondrial biogenesis and allowed tumor cells to adapt to hypoxic stress.

RESULTS

Hypoxia-Induced PGC-1α K224 Monomethylation Suppresses Mitochondrial Biogenesis in Tumor Cells

To determine the effect of hypoxia on mitochondrial biogenesis, we examined the amount of mtDNA in U87 (Figure 1A) and T98G human glioblastoma (GBM) cells, MDA-MB-231 human breast cancer cells, and BxPC-3 human pancreatic cancer cells (Figure S1A) in response to hypoxic (1% oxygen) stimulation. The amounts of mtDNA D-Loop structure and *MT-CO2* gene, which encodes for mtDNA-encoded cytochrome C oxidase II (MT-CO2), were reduced under hypoxic conditions. Hypoxia induces autophagy and the subsequent lysosomal degradation of damaged mitochondria and mitochondrial components, which is known as mitophagy (White, 2012). Pretreatment of cells with the lysosomal inhibitor chloroquine diphosphate (CQ) (Figure S1B) or deficiency of *Atg5* (Figure S1C), which blocked autophagy- and lysosome-mediated degradation of LC3B-II and p62, only partially abrogated the hypoxia-mediated downregulation of mtDNA (Figures 1A, S1A, and S1D) and the mtDNA-encoded expression of MT-CO2 and cytochrome B (MT-CYB) (Figures 1B and S1E). In addition, U87 cells with CRISPR/Cas9-created indel mutations (insertion and deletion) of *ATG5* autophagy gene (Figure S1F), which successfully deleted ATG5 expression and blocked autophagy (Figure S1G), exhibited similar results (Figures S1H and S1I) and only partially rescued hypoxia-reduced total mitochondrial contents (Figure 1C). These results strongly suggest that hypoxia suppresses the mitochondrial biogenesis of tumor cells, which is independent of hypoxia-induced mitophagy.

To determine whether hypoxia regulates PGC-1α, a key player in mitochondrial biogenesis, we examined the expression of PGC-1α. We did not detect obvious changes of the mRNA

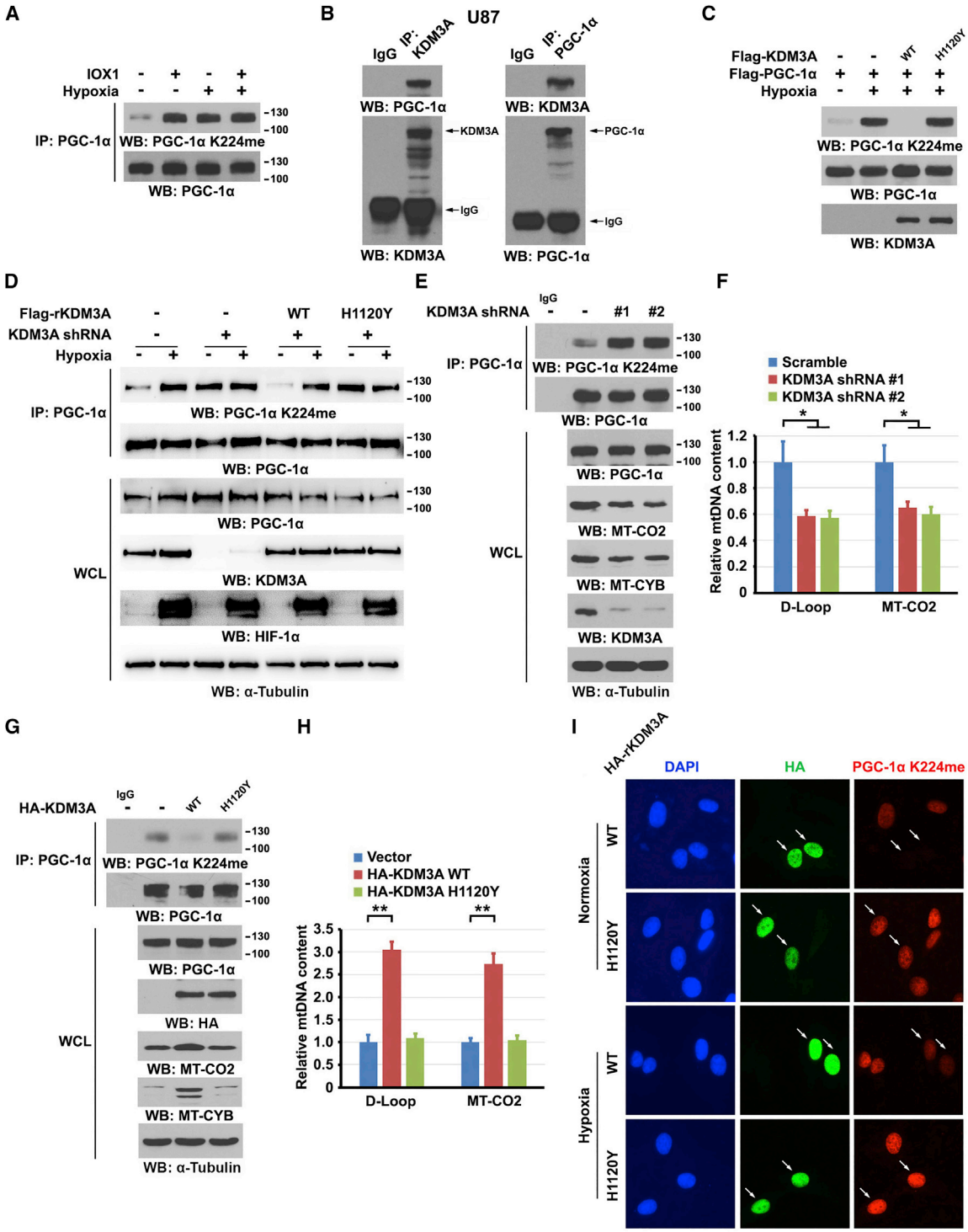

Figure 2. PGC-1α K224 Monomethylation Is Demethylated by KDM3A

(A) U87 cells were pretreated with or without 200 μM IOX1 for 12 h, followed by treatment with or without hypoxia for 12 h. Immunoblotting analyses were performed.

(B) U87 cells were lysed. Immunoprecipitation was performed by incubating the indicated antibodies (10 μg) with 1 mg of cell lysates at 4°C for overnight, followed by incubation of protein G-agarose beads for 3 h. The beads were then washed with a lysis buffer for 4 times.

(C) FLAG-PGC-1α was purified from U87 cells in the presence or absence of hypoxia, followed by incubation with WT FLAG-KDM3A or FLAG-KDM3A H1120Y mutant purified from 293T cells. An *in vitro* demethylation assay was performed.

(legend continued on next page)

(Figure S2A) or protein expression (Figure S2B) of PGC-1α upon hypoxic stimulation (1% O_2). We next determined whether PGC-1α is posttranslationally modified, thereby altering PGC-1α's activity. Immunoprecipitation of FLAG-tagged PGC-1α from hypoxia-stimulated U87 cells, followed by liquid chromatography-tandem mass spectrometry, revealed that PGC-1α is monomethylated at evolutionally conserved K224 (Figures S2C and S2D). In addition, immunoblotting analyses with an anti-monomethylated K224 of PGC-1α antibody, which detected monomethylated, but not di- or tri-methylated, K224 of PGC-1α peptides (Figure S2E), showed that PGC-1α K224 was limitedly monomethylated under a normoxic condition (Figure 1D) and that hypoxic stimulation induced this monomethylation in U87 (Figure 1D), U251, T98G, and HeLa cells (Figure S2F).

Reconstituted expression of short hairpin RNA (shRNA)-resistant (r) PGC-1α K224R mutant, which was resistant to be monomethylated at K224 (Figure S2G), in U87 cells with ATG5 deficiency (Figure S2H), blocked hypoxia-reduced mtDNA (Figure 1E), the expression of MT-CO2 and MT-CYB (Figure 1F), and the total mitochondrial contents (Figure 1G). Of note, a similar effect was also observed in normal human astrocytes (NHAs) (Figure S2I), suggesting a shared regulation of PGC-1α between normal and tumor cells under hypoxic conditions. Under a near anoxia (0.2% O_2) condition, we detected upregulated PGC-1α expression (Arany et al., 2008) in U87 cells with correspondingly enhanced K224 monomethylation (Figure S2J). However, the amounts of mtDNA under this condition were comparably suppressed to that under 1% O_2 stimulation (Figure S2K), suggesting that K224 monomethylation, but not expression level, of PGC-1α plays a role for suppressed mtDNA synthesis under low O_2 conditions.

To determine whether hypoxia-reduced mtDNA is HIF-1α-dependent, we depleted HIF-1α in U87 cells by expressing HIF-1α shRNA (Figure S2L). Depletion of HIF-1α in U87 cells had no effect on hypoxia-induced PGC-1α K224 monomethylation (Figure S2L), PGC-1β mRNA expression (Figure S2M), or mtDNA contents (Figure S2N). These results suggest that hypoxia-induced monomethylation of PGC-1α K224 suppresses the mitochondrial biogenesis in a HIF-1α-independent manner.

PGC-1α K224 Monomethylation Is Demethylated by KDM3A

To determine whether hypoxia-induced monomethylation of PGC-1α K224 is regulated by a demethylase, we treated U87 cells with 5-carboxy-8-hydroxyquinoline (IOX1), a potent broad-spectrum inhibitor of the JMJD family of 2-oxoglutarate-dependent demethylases, or deferoxamine (DFO), an iron chelator that blocks iron-dependent demethylation. Both IOX1 (Figure 2A) and DFO (Figure S3A) treatment substantially increased PGC-1α K224 monomethylation, and this was not further enhanced by hypoxic stimulation, suggesting that PGC-1α K224 monomethylation induced by hypoxia is due to inhibition of a demethylase. Immunoprecipitation of FLAG-tagged KDMs in 293T cells showed that only KDM3A interacted with hemagglutinin (HA)-tagged PGC-1α (Figure S3B). Reciprocal immunoprecipitation showed that endogenous PGC-1α interacted with endogenous KDM3A in U87 (Figure 2B) and T98G (Figure S3C) cells. Expression of PGC-1α truncation mutants revealed that C-terminal half of PGC-1α (amino acids 404–798) is important for PGC-1α's binding to KDM3A (Figures S3D and S3E). In addition, we showed that serine/arginine-rich (SR) region, but not RNA recognition motif (RRM), in the C terminus of PGC-1α interacted with KDM3A (Figure S3E). Expression of PGC-1α mutant with SR deletion (ΔSR) increased K224 monomethylation under a normoxic condition (Figure S3F). These results indicate that SR region of PGC-1α interacts with KDM3A and regulates K224 monomethylation of PGC-1α.

To support the finding that KDM3A regulates PGC-1α K224 monomethylation, we incubated purified active wild-type (WT) KDM3A, inactive KDM3A H1120Y mutant (Figure S3G), or purified active KDM2A or KDM4A with immunoprecipitated PGC-1α from hypoxia-stimulated U87 cells. We showed that only WT KDM3A demethylated monomethylated K224 of PGC-1α (Figures 2C, S3H, and S3I). Reconstituted expression of shRNA-resistant (r) WT KDM3A or rKDM3A H1120Y in endogenous KDM3A-depleted U87 cells (Figure 2D) and NHA (Figures S3J and S3K) showed that KDM3A depletion or rKDM3A H1120Y expression, in contrast to parental cells or reconstituted expression of WT rKDM3A, substantially increased PGC-1α K224 monomethylation under normoxic conditions; this increase was not further enhanced by hypoxic stimulation (Figures 2D and S3K). In line with these findings, KDM3A depletion reduced the expression of MT-CO2 and MT-CYB (Figure 2E), which was accompanied by the reduction in the amounts of mtDNA D-loop structure and *MT-CO2* gene (Figure 2F). In contrast, overexpression of WT KDM3A, but not KDM3A H1120Y, in U87 cells demethylated monomethylated K224 of PGC-1α, increased the expression of MT-CO2 and MT-CYB (Figure 2G) and mtDNA amounts (Figure 2H). Notably, immunofluorescent studies showed that WT KDM3A, but not KDM3A H1120Y, suppressed nucleus-localized PGC-1α K224 monomethylation and that this suppression was partially rescued by hypoxic stimulation (Figures 2I and S3L). To further validate the cellular regulation of PGC-1α K224 monomethylation by KDM3A, we established CRISPR/Cas9-mediated knockin expression of KDM3A H1120Y mutant in U87 cells and observed enhanced effect on

(D) U87 cells with or without depleted KDM3A and reconstituted expression of WT FLAG-rKDM3A or FLAG-rKDM3A H1120Y mutant were treated with or without hypoxia for 12 h.

(E and F) U87 cells with depleted KDM3A were cultured. Immunoprecipitation and immunoblotting analyses (E) and qPCR analyses (F) were performed.

(G and H) U87 cells with or without expression of WT HA-KDM3A or HA-KDM3A H1120Y mutant were cultured. Immunoprecipitation and immunoblotting analyses (G) and qPCR analyses (H) were performed.

(I) U87 cells with depleted KDM3A and reconstituted expression of WT HA-rKDM3A or HA-rKDM3A H1120Y mutant were treated with or without hypoxia for 12 h. Immunofluorescence was performed with the indicated antibodies. White arrows indicate KDM3A-positive nuclei.

(A–E and G) Immunoprecipitation and immunoblotting analyses were performed with the indicated antibodies. (F and H) Data represent the mean ± SD from triplicate experiments. *$p < 0.05$; **$p < 0.001$. See also Figure S3.

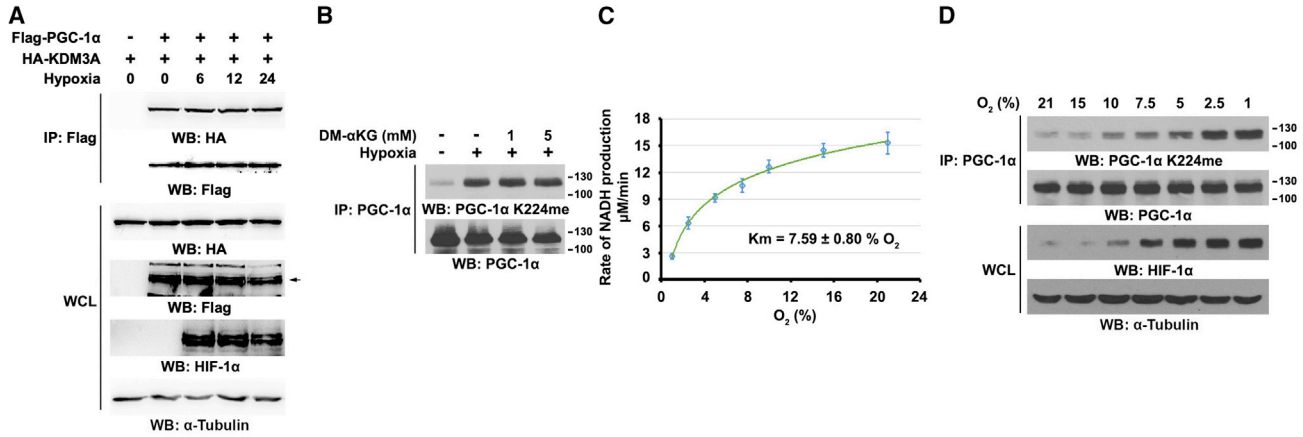

Figure 3. KDM3A Senses Oxygen Availability to Regulate PGC-1α K224 Monomethylation

(A) U87 cells expressing HA-KDM3A with or without FLAG-PGC-1α were treated with hypoxia for the indicated periods of time. Immunoprecipitation and immunoblotting analyses were performed with the indicated antibodies.

(B) U87 cells treated with or without the indicated concentrations of DM-αKG were cultured with or without hypoxia for 12 h. Immunoprecipitation and immunoblotting analyses were performed with the indicated antibodies.

(C) Michaelis-Menten curve of KDM3A for oxygen. Reactions were performed by mixing purified active KDM3A and K224-monomethylated PGC-1α peptide under the indicated oxygen tensions. *K*m denotes the Michaelis constant. Data represent the mean ± SD from triplicate experiments.

(D) U87 cells were cultured under the indicated oxygen concentrations for 12 h. Immunoprecipitation and immunoblotting analyses were performed with the indicated antibodies.

PGC-1α K224 monomethylation (Figure S3M) and reduced mtDNA amounts (Figure S3N). These results indicate that PGC-1α K224 monomethylation is demethylated by KDM3A and that hypoxia inhibits this demethylation, leading to inhibited mitochondrial biogenesis.

KDM3A Senses Oxygen Availability to Regulate PGC-1α K224 Monomethylation

To identify the mechanism underlying KDM3A-regulated PGC-1α K224 monomethylation, we determined whether hypoxia regulates the binding of KDM3A to PGC-1α. U87 cells were transfected with FLAG-PGC-1α and HA-KDM3A. Immunoprecipitation analyses showed that hypoxia did not alter the association between HA-KDM3A and PGC-1α (Figure 3A). We next determined whether KDM3A's activity is regulated by hypoxia, thereby modulating PGC-1α K224 monomethylation. It is known that α-ketoglutarate (αKG)-dependent demethylases require αKG and oxygen for their activity (Kooistra and Helin, 2012). To determine whether hypoxia-inhibited KDM3A is due to a deficiency of αKG, we supplied U87 cells with different dosages of cell-membrane-permeable dimethyl (DM)-αKG. We did not detect an obvious reduction in PGC-1α K224 monomethylation under hypoxia (Figure 3B), suggesting that hypoxia-regulated KDM3A is not caused by an alteration of αKG levels. We next determined the K_M of oxygen for KDM3A activity toward demethylating PGC-1α K224 monomethylation. We showed that this K_M was relatively high (about 7.6% oxygen; Figure 3C), suggesting that this activity is sensitive to oxygen concentration changes. As expected, PGC-1α K224 monomethylation exhibited a dynamic response to the availability of oxygen to U87 cells; this monomethylation was substantially increased when oxygen tension was dropped below 5% (Figure 3D). These results indicate that KDM3A senses oxygen availability and regulates the cellular response to hypoxia by directly regulating PGC-1α monomethylation-dependent mitochondrial biogenesis.

PGC-1α K224 Monomethylation Inhibits PGC-1α-Mediated NRF1/2 Activation and Inhibits Mitochondrial Biogenesis

To identify the effect of PGC-1α K224 monomethylation on PGC-1α activity, we performed co-immunoprecipitation analyses to determine whether hypoxia regulates the binding of PGC-1α to its co-activated transcription factors (Lin et al., 2005; Scarpulla et al., 2012). Hypoxic stimulation resulted in reduced binding of WT rPGC-1α, which was expressed in endogenous PGC-1α-depleted U87 cells (Figure S4A), to NRF1 and NRF2α (Figure 4A), but not to ERRα, PPARα, or YY1 (Figures S4B–S4D). In contrast, reconstituted expression of rPGC-1α K224R, which by itself increased its binding to NRF1/2, was resistant to hypoxia-reduced interaction of these proteins (Figure 4A).

We next performed *in vitro* pull-down analyses by incubating U87 cell-purified FLAG-PGC-1α (Figures S4E and S4F) with 293T cell-purified HA-NRF1 (Figure S4G) or HA-host cell factor 1 (HCF1) (Figure S4H), which was reported to bridge the binding of PGC-1α to NRF2 (Vercauteren et al., 2008). Hypoxia-induced PGC-1α K224 monomethylation abrogated the direct binding of PGC-1α to NRF1 or HCF1, and the interaction between PGC-1α K224R and NRF1 or HCF1 was not altered by hypoxic stimulation (Figures S4I and S4J). Chromatin immunoprecipitation assays showed that WT PGC-1α, but not PGC-1α K224R, reduced the localization of PGC-1α at the promoter regions of NRF1/2-downstream genes, *TFAM*, *TFB1M*, and *TFB2M*, upon hypoxic stimulation and that PGC-1α K224R had enhanced accumulation at these promoter regions under both normoxic and hypoxic conditions (Figure 4B).

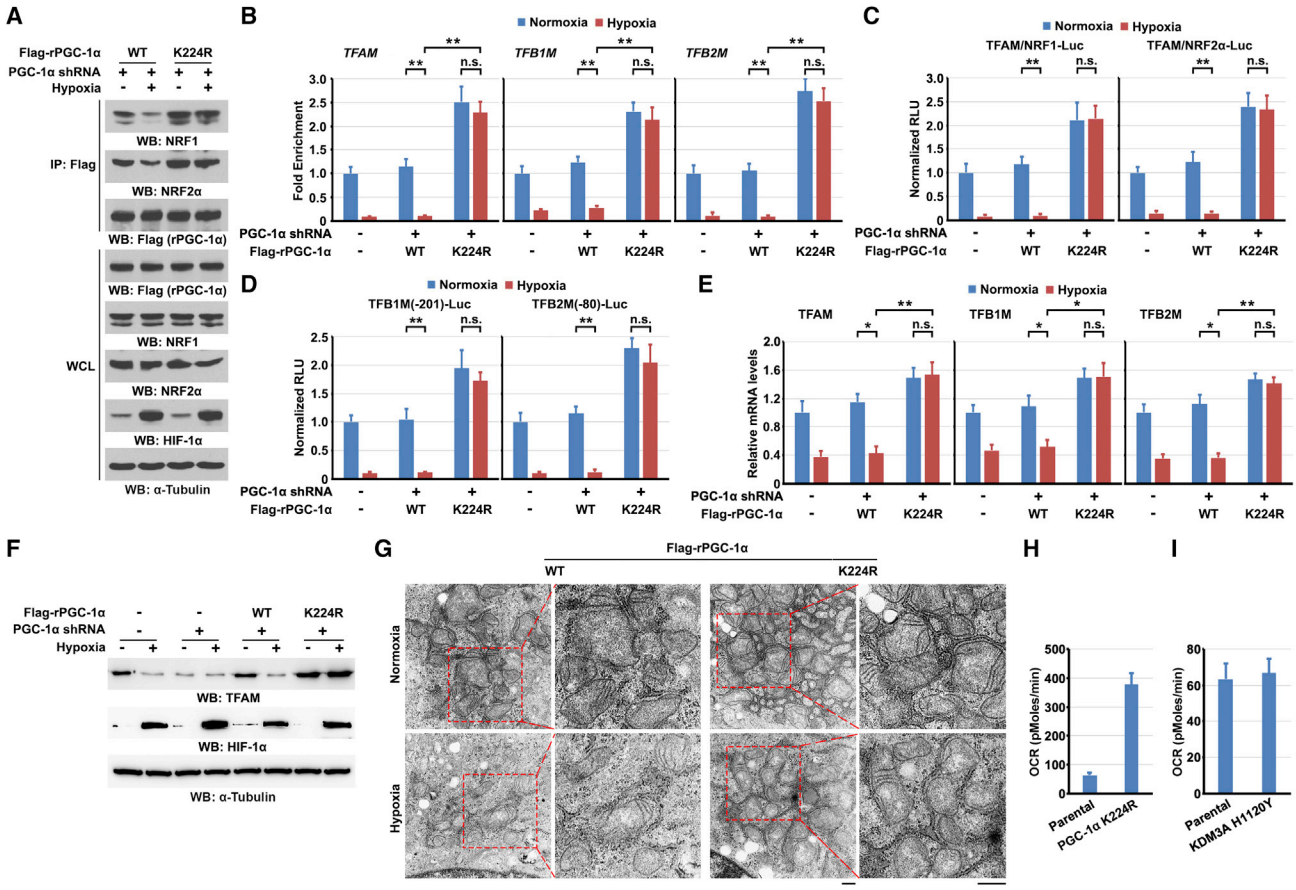

Figure 4. PGC-1α K224 Monomethylation Inhibits PGC-1α-Mediated NRF1/2 Activation and Inhibits Mitochondrial Biogenesis

(A and B) U87 cells with or without depleted PGC-1α and with reconstituted expression of WT FLAG-rPGC-1α or FLAG-rPGC-1α K224R were treated with or without hypoxia for 24 h.

(A) Immunoprecipitation and immunoblotting assays were performed with the indicated antibodies.

(B) Chromatin immunoprecipitation (ChIP) analyses with an anti-FLAG antibody and PCR with primers against *TFAM* (left), *TFB1M* (middle), or *TFB2M* (right) promoter region were performed.

(C and D) U87 cells with or without depleted PGC-1α and reconstituted expression of WT FLAG-rPGC-1α or FLAG-rPGC-1α K224R were transfected with TFAM/NRF1-Luc (C; left panel), TFAM/NRF2α-Luc (C; right panel), TFB1M(−201)-Luc (D; left panel), or TFB2M(−80)-Luc (D; right panel), followed by treatment with or without hypoxia for 24 h. Luciferase activities were measured.

(E) U87 cells with or without depleted PGC-1α and reconstituted expression of WT FLAG-rPGC-1α or FLAG-rPGC-1α K224R were treated with or without hypoxia for 24 h. qRT-PCR analyses were performed with primers against TFAM (left panel), TFB1M (middle panel), or TFB2M (right panel).

(F) U87 cells with or without depleted PGC-1α and reconstituted expression of WT FLAG-rPGC-1α or FLAG-rPGC-1α K224R were treated with or without hypoxia for 24 h. Immunoprecipitation and immunoblotting assays were performed with the indicated antibodies.

(G) ATG5-null U87 cells with depleted PGC-1α and reconstituted expression of WT FLAG-rPGC-1α or FLAG-rPGC-1α K224R were treated with or without hypoxia for 24 h. Electron microscopic analyses were performed. Scale bar, 500 nm.

(H and I) Measurement of oxygen consumption rate (OCR). Parental U87 cells or U87 cells with PGC-1α K224R knockin (H) or KDM3A H1120Y knockin (I) expression were cultured for measuring OCRs using oxygen electrode under hypoxic conditions. Data represent the mean ± SD from triplicate experiments.

(B–E) Data represent the mean ± SD from triplicate experiments. *$p < 0.05$; **$p < 0.001$; n.s., no significance. See also Figure S4.

To determine the effect of PGC-1α K224 monomethylation on the transcriptional activity of NRF1/2, we expressed luciferase reporters driven by NRF1/2-binding promoter regions of *TFAM* (Wu et al., 1999), *TFB1M*, and *TFB2M* (Gleyzer et al., 2005) in U87 cells. Hypoxic stimulation suppressed the NRF1/2-regulated promoter activities (Figures 4C and 4D) and corresponding mRNA levels (Figure 4E) of these genes. In contrast, reconstituted expression of rPGC-1α K224R increased the promoter activities (Figures 4C and 4D) and mRNA levels (Figure 4E) of these genes and enabled these promoters to become resistant to hypoxia-induced suppression. In line with these results, hypoxia-repressed expression of TFAM was abrogated by reconstituted expression of PGC-1α K224R in U87 (Figure 4F) and T98G cells (Figure S4K) or knockin expression of PGC-1α K224R mutant in U87 cells (Figure S4L). We next performed electronic microscopy analyses and showed that hypoxia reduced the total number of mitochondria in ATG5-null U87 cells with reconstituted expression of WT rPGC-1α (Figures 4G and S4M). However,

the reduction was abrogated in cells expressing rPGC-1α K224R.

To determine the effect of PGC-1α K224 monomethylation on mitochondrial functions, we measured mitochondrial oxygen consumption rate (OCR). Knockin expression of PGC-1α K224R in U87 cells only slightly increased OCRs under normoxic conditions (Figure S4N); this limited change is likely due to low levels of PGC-1α K224 monomethylation in the presence of ample O_2 (Figure 1D). In contrast, under hypoxic conditions, OCRs in U87 cells with knockin expression of PGC-1α K224R were significantly higher than those in parental cells expressing WT PGC-1α (Figure 4H). In addition, knockin expression of KDM3A H1120Y in U87 cells, which substantially increased PGC-1α K224 monomethylation (Figure S3M), decreased OCRs under normoxic, but not hypoxic, conditions (Figures 4I and S4O). All together, these results indicate that KDM3A-mediated PGC-1α K224 monomethylation reduces the transcriptional activity of NRF1 or NRF2 for *TFAM*, *TFB1M*, and *TFB2M* expression, leading to inhibited mitochondrial biogenesis and functions.

PGC-1α K224 Monomethylation Reduces ROS Production and Apoptosis and Promotes Tumor Growth

Hypoxia enhances reactive oxygen species (ROS) production, in which mitochondrial activity plays an important role (Li et al., 2016b). As expected, hypoxic stimulation-induced ROS production (Figure 5A), cleavage of PARP by activated caspases (Figure S5A), and cell apoptosis (Figure 5B) in U87 cells with depletion of endogenous PGC-1α and reconstituted expression of WT rPGC-1α were substantially augmented by the reconstituted expression of rPGC-1α K224R mutant (Figures 5A, 5B, and S5A). Treatment of PGC-1α K224R-expressing U87 cells with the thiol-reducing agent N-acetylcysteine (NAC) partially reduced intracellular ROS levels (Figure 5A) and cell apoptosis (Figure 5B) under hypoxic conditions. Consistent with rPGC-1α K224R-enhanced ROS production, expression of anti-oxidative genes, such as *SOD2*, *GPX1*, *TXN2*, and *TXNDC14* (Luo et al., 2017; Vazquez et al., 2013), was increased in U87 cells expressing rPGC-1α K224R (Figure S5B), suggesting an adaptive response of these cells to ROS production, although this response failed to curb the overall ROS production. As expected, the increase of these gene expressions was reduced by NAC treatment, suggesting that K224 monomethylation of PGC-1α regulates ROS production and subsequently anti-oxidant gene expression. We next performed cell counting analyses and showed that rPGC-1α K224R expression, which did not alter cell proliferation under normoxic condition (Figure S5C), further decreased hypoxia-suppressed cell proliferation (Figure 5C). These results indicate that PGC-1α K224 monomethylation plays an important role in regulating ROS production and promotes cell survival in response to hypoxic stimulation.

To determine the role of PGC-1α K224 monomethylation in brain tumor development, we intracranially injected athymic nude mice with U87 cells with depleted endogenous PGC-1α and reconstituted expression of WT PGC-1α or PGC-1α K224R mutant. Compared to WT PGC-1α expression, PGC-1α K224R mutant expression failed to rescue PGC-1α depletion-impaired tumor growth (Figures 5D and S5D) that was accompanied by non-detectable PGC-1α K224 monomethylation (Figure S5E), low levels of Ki-67 expression reflecting inhibited cell proliferation (Figures 5E and S5F), and increased cell apoptosis in tumor tissues (Figures 5F and S5G). In addition, we exposed mice in 11% low-oxygen tension. Compared with a normoxic condition, 11% oxygen exposure resulted in a reduced brain tumor growth (Figures 5G and S5H) with correspondingly enhanced PGC-1α K224 monomethylation in tumors (Figures 5H and S5I) with U87 parental cells injection. Notably, the low oxygen condition induced further inhibition of tumor growth in mouse with injection of U87 cells harboring PGC-1α K224R knockin expression (Figures 5G and S5H). These results suggest that KDM3A-mediated PGC-1α K224 monomethylation counteracts hypoxic stress to promote tumor growth.

To determine the clinical significance of hypoxic stress on PGC-1α K224 monomethylation, we performed immunohistochemistry (IHC) analyses in 50 human primary GBM specimens. We showed that PGC-1α K224 monomethylation levels, but not total levels of PGC-1α expression, were positively correlated with hypoxic marker HIF-1α expression (Figure 5I). Quantification of the IHC staining demonstrated that this correlation was significant (Figure 5J). These results highlighted the clinical significance of PGC-1α K224 monomethylation in tumor development.

DISCUSSION

The maintenance of oxygen homeostasis is essential for the survival of most prokaryotic and eukaryotic species. Oxygen deprivation (hypoxia), which occurs during solid tumor growth, triggers complex adaptive responses to match the oxygen supply with the metabolic and bioenergetic demands (Nakazawa et al., 2016). Although suppressed mitochondrial function under hypoxic conditions has been extensively reported, most studies have been focused on the HIF-1α-dependent regulation, including upregulated expression of pyruvate dehydrogenase kinase 1 (PGK1) (Kim et al., 2006; Papandreou et al., 2006) and NDUFA4 mitochondrial complex associated like 2 (NDUFA4L2) (Tello et al., 2011) and c-Myc degradation-dependent downregulation of PGC-1β (Zhang et al., 2007). PGC-1α is a key regulator of mitochondrial biogenesis and oxidative metabolism. However, how PGC-1α is posttranslationally regulated in response to oxygen availability remains largely unclear. We demonstrated here that KDM3A is an oxygen sensor acting like recently reported KDM5A and KDM6A, which sense O_2 availability to regulate histone methylation and gene expression (Batie et al., 2019; Chakraborty et al., 2019). KDM3A interacted with PGC-1α and demethylated monomethylated K224 of PGC-1α. Oxygen deficiency resulted in inhibition of KDM3A, which had a high K_M for its activity and was dynamically regulated by oxygen availability, leading to enhanced monomethylation of PGC-1α K224 in a HIF-1α-independent manner. Lysine methylation regulates protein-protein interactions (Hamamoto et al., 2015). Monomethylation of PGC-1α K224, which may alter PGC-1α conformation, reduced the binding of PGC-1α to NRF1/2 and subsequent NRF1- and NRF2-dependent expression of *TFAM*, *TFB1M*, and *TFB2M*; these effects resulted in reduced mitochondrial biogenesis, which was reflected by reductions in

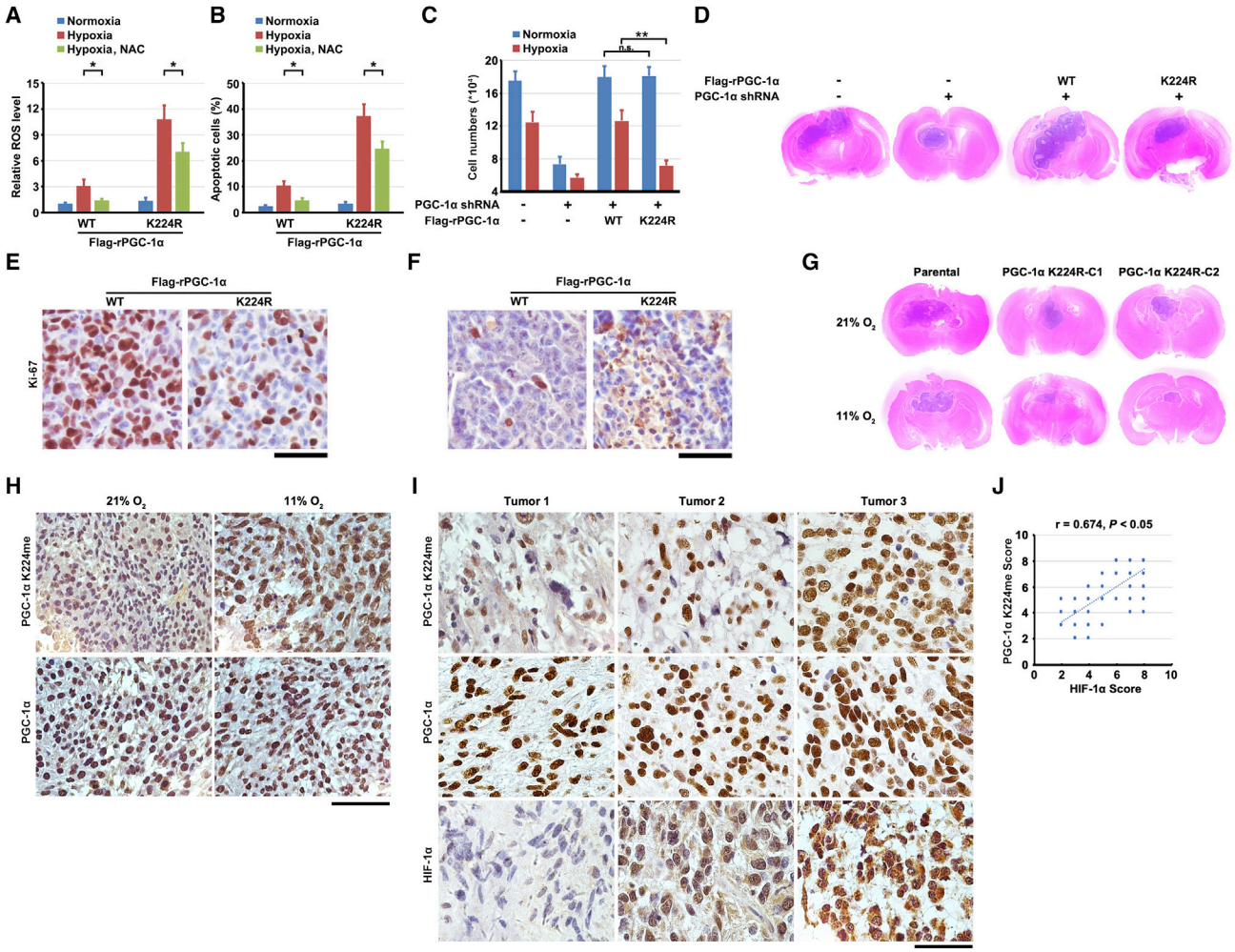

Figure 5. PGC-1α K224 Monomethylation Reduces ROS Production and Apoptosis and Promotes Tumor Growth

(A and B) U87 cells depleted with PGC-1α and with reconstituted expression of WT FLAG-rPGC-1α or FLAG-rPGC-1α K224R were treated with or without hypoxia for 24 h in the presence or absence of N-acetyl-L-cysteine (NAC) (2 mM). ROS levels (A) and apoptotic cells (B) were measured. Data represent the mean ± SD from triplicate experiments. *$p < 0.05$.

(C) U87 cells (4×10^4) with or without depleted PGC-1α and with reconstituted expression of WT FLAG-rPGC-1α or FLAG-rPGC-1α K224R were cultured for 3 days. Cell numbers were counted. Data represent the mean ± SD of triplicate samples. **$p < 0.001$.

(D–F) U87 cells with or without depleted PGC-1α and with reconstituted expression of WT FLAG-rPGC-1α or FLAG-rPGC-1α K224R were intracranially injected into athymic nude mice (n = 7 per group). Mice were sacrificed for examination of tumor growth.

(D) Representative H&E-stained coronal brain sections are shown.

(E) Immunohistochemical analyses of xenograft brain tumor tissues were performed with an anti-Ki-67 antibody.

(F) TUNEL analyses of the indicated tumor tissues were performed. Apoptotic cells were stained brown.

(G and H) Mice were intracranially injected with U87 cells or U87 cells with PGC-1α K224R knockin expression. Mice were put in ambient atmosphere (21% O_2) or 11% oxygen tension for 28 days after injection and sacrificed for examination of tumor growth.

(G) Representative H&E-stained coronal brain sections are shown.

(H) Immunohistochemical analyses of brain tumor tissues derived from parental U87 cells were performed with the indicated antibodies. Scale bar, 50 μm.

(I and J) Human GBM samples were immunohistochemically stained with the indicated antibodies.

(I) Representative images are shown.

(J) The Pearson correlation test was used. Of note is that some of the dots on the graphs represent more than one sample (i.e., some scores overlapped).

See also Figure S5.

mtDNA, mitochondrial contents, and the total number of mitochondria (Figure 6). Abrogation of the monomethylation of PGC-1α K224 through the expression of PGC-1α K224R mutant significantly increased ROS production and tumor cell apoptosis and inhibited brain tumor growth in mice. These findings revealed an instrumental regulation of mitochondrial functions, in which oxygen sensing by KDM3A-mediated PGC-1α K224 monomethylation plays a critical role.

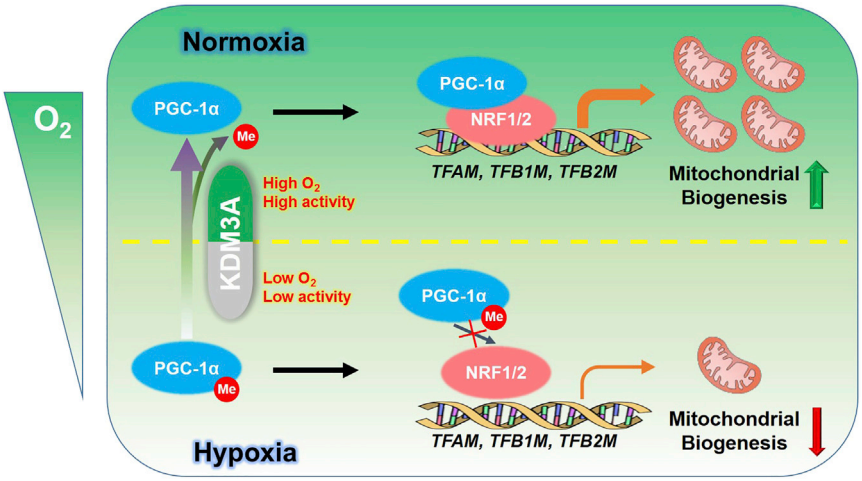

Figure 6. A Schematic Model Showing that Hypoxia-Induced PGC-1α K224 Monomethylation Suppresses Mitochondrial Biogenesis

The coupling of mitochondrial biogenesis with expression of mitochondrial proteins encoded by the nuclear genome is proposed to be regulated by nucleus-to-mitochondria "anterograde" and mitochondrion-to-nucleus "retrograde" signaling (Quirós et al., 2016). KDM3A-mediated PGC-1α K224 monomethylation acts as an anterograde regulation of mitochondrial biogenesis in response to hypoxic stress. In response to the anterograde signaling, mitochondria can control the expression of nuclear genes through a "retrograde" signaling, as exampled by yeast mtDNA depletion-induced nuclear translocation of cytosolic Rtg1p/3p complex for expression of the genes that encode mitochondrial proteins (Sekito et al., 2000; Traven et al., 2001). Upon mitochondrial depolarization commonly induced by hypoxia in GBM cells (Turcotte et al., 2002), transcriptional cofactor G protein pathway suppressor 2 (GPS2) was translocated from mitochondria to the nucleus, where GPS2 bound to the promoters of genome-encoded mitochondrial genes and regulated their expression (Cardamone et al., 2018). In addition, it was shown that TFAM knockdown enhanced α-ketoglutarate (αKG) levels, thereby activating αKG-dependent prolyl hydroxylase domain-containing protein 2 (PHD2) for inhibiting HIF1α- and Wnt/β-catenin signaling-promoted mitochondrial protein expression and mitochondrial biogenesis (Vergara et al., 2017; Wen et al., 2019). Thus, our results, together with others from previous publications, suggest that PGC-1α K224 monomethylation-mediated anterograde signaling, including reduction of TFAM, subsequently affect TFAM- and others-induced retrograde signaling for a balanced mitochondrial biogenesis.

Cancer cells under hypoxic or ischemic conditions use oxygen-sensing pathways to adapt to microenvironmental stresses. Although PGC-1α is posttranslationally modified in a signaling context-dependent manner (Fernandez-Marcos and Auwerx, 2011; Scarpulla et al., 2012), its regulation in response to oxygen availability remains largely elusive. Our findings elucidated a novel and important mechanism underlying the hypoxia-induced inhibition of PGC-1α and subsequent mitochondrial biogenesis, which is through inhibiting KDM3A-mediated demethylation of monomethylated K224 of PGC-1α. Inhibition of PGC-1α K224 monomethylation largely blocked brain tumor development, highlighting the potential to disrupt PGC-1α K224 regulation as an alternative approach to cancer.

STAR★METHODS

Detailed methods are provided in the online version of this paper and include the following:

- KEY RESOURCES TABLE
- LEAD CONTACT AND MATERIALS AVAILABILITY
- EXPERIMENTAL MODEL AND SUBJECT DETAILS
  - Mice
  - Human subjects and immunohistochemical staining
  - Cell culture and hypoxia treatment
- METHOD DETAILS
  - Materials
  - DNA construction and mutagenesis
  - Transfection
  - CRISPR/Cas9-mediated genomic editing
  - Measurement of mitochondrial DNA content
  - Assessment of mitochondrial content
  - Measurement of intracellular ROS
  - Apoptosis analysis
  - Cell viability analyses
  - Cell proliferation analyses
  - Immunoprecipitation and immunoblotting assay
  - Immunofluorescent analyses
  - Mass spectrometry
  - qRT-PCR
  - *In vitro* demethylation assay
  - Measurement of oxygen consumption rate (OCR)
  - Km determination
  - Luciferase assay
  - ChIP assay
  - Transmission electron microscopy
- QUANTIFICATION AND STATISTICAL ANALYSIS
- DATA AND CODE AVAILABILITY

SUPPLEMENTAL INFORMATION

Supplemental Information can be found online at https://doi.org/10.1016/j.molcel.2019.09.019.

ACKNOWLEDGMENTS

We thank Dr. Li Li (Clinical and Translational Proteomics Service Center, Institute of Molecular Medicine, The University of Texas Health Center at Houston) for MS spectrometry assistance and Mr. Kenneth Dunner, Jr. (High Resolution Electron Microscopy Facility of MD Anderson Cancer Center with the support of CCSG grant NIH P30 CA016672) for electronic microscopy assistance. This work was supported by Start Funding KY103RC20190002 and Science and Technology Development Fund of Nanjing Medical University JX218317201711010 (to X.Q.), Key Program of the Chinese Academy of Sciences KJZD-SW-L05 (to X.L.), and National Natural Science Foundation of China 81772951 (to Z.S.) and 81772679 (to Y.Y.). Z.L. is a Kuancheng Wang Distinguished Chair.

AUTHOR CONTRIBUTIONS

This study was conceived and designed by Z.L. and X.Q. X.Q., X.L., Z.S., X.B., Y.X., Y.Z., and D.X. performed experiments. F.C., Y.Y., Z.H., and Q.Z. provided reagents and technical support. Z.L. wrote the paper with comments from all authors.

DECLARATION OF INTERESTS

Z.L. owns shares in Signalway Biotechnology (Pearland, TX), which supplied the rabbit antibody that recognizes PGC-1α K224 monomethylation. Z.L.'s interest in this company had no bearing on its being chosen to supply this reagent.

Received: July 25, 2018
Revised: July 22, 2019
Accepted: September 12, 2019
Published: October 16, 2019

REFERENCES

Andrzejewski, S., Klimcakova, E., Johnson, R.M., Tabariès, S., Annis, M.G., McGuirk, S., Northey, J.J., Chénard, V., Sriram, U., Papadopoli, D.J., et al. (2017). PGC-1α promotes breast cancer metastasis and confers bioenergetic flexibility against metabolic drugs. Cell Metab *26*, 778–787.e5.

Arany, Z., Foo, S.Y., Ma, Y., Ruas, J.L., Bommi-Reddy, A., Girnun, G., Cooper, M., Laznik, D., Chinsomboon, J., Rangwala, S.M., et al. (2008). HIF-independent regulation of VEGF and angiogenesis by the transcriptional coactivator PGC-1alpha. Nature *451*, 1008–1012.

Batie, M., Frost, J., Frost, M., Wilson, J.W., Schofield, P., and Rocha, S. (2019). Hypoxia induces rapid changes to histone methylation and reprograms chromatin. Science *363*, 1222–1226.

Cardamone, M.D., Tanasa, B., Cederquist, C.T., Huang, J., Mahdaviani, K., Li, W., Rosenfeld, M.G., Liesa, M., and Perissi, V. (2018). Mitochondrial retrograde signaling in mammals is mediated by the transcriptional cofactor GPS2 via direct mitochondria-to-nucleus translocation. Mol. Cell *69*, 757–772.e7.

Chakraborty, A.A., Laukka, T., Myllykoski, M., Ringel, A.E., Booker, M.A., Tolstorukov, M.Y., Meng, Y.J., Meier, S.R., Jennings, R.B., Creech, A.L., et al. (2019). Histone demethylase KDM6A directly senses oxygen to control chromatin and cell fate. Science *363*, 1217–1222.

Cunningham, J.T., Rodgers, J.T., Arlow, D.H., Vazquez, F., Mootha, V.K., and Puigserver, P. (2007). mTOR controls mitochondrial oxidative function through a YY1-PGC-1alpha transcriptional complex. Nature *450*, 736–740.

Fang, D., Hawke, D., Zheng, Y., Xia, Y., Meisenhelder, J., Nika, H., Mills, G.B., Kobayashi, R., Hunter, T., and Lu, Z. (2007). Phosphorylation of beta-catenin by AKT promotes beta-catenin transcriptional activity. J. Biol. Chem. *282*, 11221–11229.

Fernandez-Marcos, P.J., and Auwerx, J. (2011). Regulation of PGC-1α, a nodal regulator of mitochondrial biogenesis. Am. J. Clin. Nutr. *93*, 884S–890S.

Gleyzer, N., Vercauteren, K., and Scarpulla, R.C. (2005). Control of mitochondrial transcription specificity factors (TFB1M and TFB2M) by nuclear respiratory factors (NRF-1 and NRF-2) and PGC-1 family coactivators. Mol. Cell. Biol. *25*, 1354–1366.

Hamamoto, R., Saloura, V., and Nakamura, Y. (2015). Critical roles of non-histone protein lysine methylation in human tumorigenesis. Nat. Rev. Cancer *15*, 110–124.

He, J., Shen, L., Wan, M., Taranova, O., Wu, H., and Zhang, Y. (2013). Kdm2b maintains murine embryonic stem cell status by recruiting PRC1 complex to CpG islands of developmental genes. Nat. Cell Biol. *15*, 373–384.

Huss, J.M., Kopp, R.P., and Kelly, D.P. (2002). Peroxisome proliferator-activated receptor coactivator-1alpha (PGC-1alpha) coactivates the cardiac-enriched nuclear receptors estrogen-related receptor-alpha and -gamma. Identification of novel leucine-rich interaction motif within PGC-1alpha. J. Biol. Chem. *277*, 40265–40274.

Jeon, S.M., Chandel, N.S., and Hay, N. (2012). AMPK regulates NADPH homeostasis to promote tumour cell survival during energy stress. Nature *485*, 661–665.

Kelly, D.P., and Scarpulla, R.C. (2004). Transcriptional regulatory circuits controlling mitochondrial biogenesis and function. Genes Dev. *18*, 357–368.

Kim, J.W., Tchernyshyov, I., Semenza, G.L., and Dang, C.V. (2006). HIF-1-mediated expression of pyruvate dehydrogenase kinase: a metabolic switch required for cellular adaptation to hypoxia. Cell Metab. *3*, 177–185.

Kooistra, S.M., and Helin, K. (2012). Molecular mechanisms and potential functions of histone demethylases. Nat. Rev. Mol. Cell Biol. *13*, 297–311.

LeBleu, V.S., O'Connell, J.T., Gonzalez Herrera, K.N., Wikman, H., Pantel, K., Haigis, M.C., de Carvalho, F.M., Damascena, A., Domingos Chinen, L.T., Rocha, R.M., et al. (2014). PGC-1α mediates mitochondrial biogenesis and oxidative phosphorylation in cancer cells to promote metastasis. Nat. Cell Biol *16*, 992–1003, 1–15.

Li, N., Dhar, S.S., Chen, T.Y., Kan, P.Y., Wei, Y., Kim, J.H., Chan, C.H., Lin, H.K., Hung, M.C., and Lee, M.G. (2016a). JARID1D is a suppressor and prognostic marker of prostate cancer invasion and metastasis. Cancer Res. *76*, 831–843.

Li, X., Jiang, Y., Meisenhelder, J., Yang, W., Hawke, D.H., Zheng, Y., Xia, Y., Aldape, K., He, J., Hunter, T., et al. (2016b). Mitochondria-translocated PGK1 functions as a protein kinase to coordinate glycolysis and the TCA cycle in tumorigenesis. Mol. Cell *61*, 705–719.

Lin, J., Handschin, C., and Spiegelman, B.M. (2005). Metabolic control through the PGC-1 family of transcription coactivators. Cell Metab. *1*, 361–370.

Liu, L., Kim, H., Casta, A., Kobayashi, Y., Shapiro, L.S., and Christiano, A.M. (2014). Hairless is a histone H3K9 demethylase. FASEB J. *28*, 1534–1542.

Lu, Z., Liu, D., Hornia, A., Devonish, W., Pagano, M., and Foster, D.A. (1998). Activation of protein kinase C triggers its ubiquitination and degradation. Mol. Cell. Biol. *18*, 839–845.

Luo, C., Lim, J.H., Lee, Y., Granter, S.R., Thomas, A., Vazquez, F., Widlund, H.R., and Puigserver, P. (2016). A PGC1α-mediated transcriptional axis suppresses melanoma metastasis. Nature *537*, 422–426.

Luo, C., Balsa, E., Thomas, A., Hatting, M., Jedrychowski, M., Gygi, S.P., Widlund, H.R., and Puigserver, P. (2017). ERRα maintains mitochondrial oxidative metabolism and constitutes an actionable target in PGC1α-elevated melanomas. Mol. Cancer Res. *15*, 1366–1375.

Matoba, S., Liu, Y., Lu, F., Iwabuchi, K.A., Shen, L., Inoue, A., and Zhang, Y. (2014). Embryonic development following somatic cell nuclear transfer impeded by persisting histone methylation. Cell *159*, 884–895.

Nakazawa, M.S., Keith, B., and Simon, M.C. (2016). Oxygen availability and metabolic adaptations. Nat. Rev. Cancer *16*, 663–673.

Osawa, T., Muramatsu, M., Wang, F., Tsuchida, R., Kodama, T., Minami, T., and Shibuya, M. (2011). Increased expression of histone demethylase JHDM1D under nutrient starvation suppresses tumor growth via down-regulating angiogenesis. Proc. Natl. Acad. Sci. USA *108*, 20725–20729.

Papandreou, I., Cairns, R.A., Fontana, L., Lim, A.L., and Denko, N.C. (2006). HIF-1 mediates adaptation to hypoxia by actively downregulating mitochondrial oxygen consumption. Cell Metab. *3*, 187–197.

Qian, X., Li, X., Cai, Q., Zhang, C., Yu, Q., Jiang, Y., Lee, J.H., Hawke, D., Wang, Y., Xia, Y., et al. (2017). Phosphoglycerate kinase 1 phosphorylates Beclin1 to induce autophagy. Mol. Cell *65*, 917–931.e6.

Qian, X., Li, X., Tan, L., Lee, J.H., Xia, Y., Cai, Q., Zheng, Y., Wang, H., Lorenzi, P.L., and Lu, Z. (2018). Conversion of PRPS hexamer to monomer by AMPK-mediated phosphorylation inhibits nucleotide synthesis in response to energy stress. Cancer Discov. *8*, 94–107.

Quirós, P.M., Mottis, A., and Auwerx, J. (2016). Mitonuclear communication in homeostasis and stress. Nat. Rev. Mol. Cell Biol. *17*, 213–226.

Ran, F.A., Hsu, P.D., Wright, J., Agarwala, V., Scott, D.A., and Zhang, F. (2013). Genome engineering using the CRISPR-Cas9 system. Nat. Protoc. *8*, 2281–2308.

Scarpulla, R.C., Vega, R.B., and Kelly, D.P. (2012). Transcriptional integration of mitochondrial biogenesis. Trends Endocrinol. Metab. *23*, 459–466.

Sekito, T., Thornton, J., and Butow, R.A. (2000). Mitochondria-to-nuclear signaling is regulated by the subcellular localization of the transcription factors Rtg1p and Rtg3p. Mol. Biol. Cell *11*, 2103–2115.

Shi, Y., Lan, F., Matson, C., Mulligan, P., Whetstine, J.R., Cole, P.A., Casero, R.A., and Shi, Y. (2004). Histone demethylation mediated by the nuclear amine oxidase homolog LSD1. Cell *119*, 941–953.

Tan, Z., Luo, X., Xiao, L., Tang, M., Bode, A.M., Dong, Z., and Cao, Y. (2016). The role of PGC1α in cancer metabolism and its therapeutic implications. Mol. Cancer Ther. *15*, 774–782.

Tello, D., Balsa, E., Acosta-Iborra, B., Fuertes-Yebra, E., Elorza, A., Ordóñez, Á., Corral-Escariz, M., Soro, I., López-Bernardo, E., Perales-Clemente, E., et al. (2011). Induction of the mitochondrial NDUFA4L2 protein by HIF-1α decreases oxygen consumption by inhibiting complex I activity. Cell Metab. *14*, 768–779.

Torrano, V., Valcarcel-Jimenez, L., Cortazar, A.R., Liu, X., Urosevic, J., Castillo-Martin, M., Fernández-Ruiz, S., Morciano, G., Caro-Maldonado, A., Guiu, M., et al. (2016). The metabolic co-regulator PGC1α suppresses prostate cancer metastasis. Nat. Cell Biol. *18*, 645–656.

Traven, A., Wong, J.M., Xu, D., Sopta, M., and Ingles, C.J. (2001). Interorganellar communication. Altered nuclear gene expression profiles in a yeast mitochondrial DNA mutant. J. Biol. Chem. *276*, 4020–4027.

Turcotte, M.L., Parliament, M., Franko, A., and Allalunis-Turner, J. (2002). Variation in mitochondrial function in hypoxia-sensitive and hypoxia-tolerant human glioma cells. Br. J. Cancer *86*, 619–624.

Vazquez, F., Lim, J.H., Chim, H., Bhalla, K., Girnun, G., Pierce, K., Clish, C.B., Granter, S.R., Widlund, H.R., Spiegelman, B.M., and Puigserver, P. (2013). PGC1α expression defines a subset of human melanoma tumors with increased mitochondrial capacity and resistance to oxidative stress. Cancer Cell *23*, 287–301.

Vega, R.B., Huss, J.M., and Kelly, D.P. (2000). The coactivator PGC-1 cooperates with peroxisome proliferator-activated receptor alpha in transcriptional control of nuclear genes encoding mitochondrial fatty acid oxidation enzymes. Mol. Cell. Biol. *20*, 1868–1876.

Vercauteren, K., Gleyzer, N., and Scarpulla, R.C. (2008). PGC-1-related coactivator complexes with HCF-1 and NRF-2beta in mediating NRF-2(GABP)-dependent respiratory gene expression. J. Biol. Chem. *283*, 12102–12111.

Vergara, D., Stanca, E., Guerra, F., Priore, P., Gaballo, A., Franck, J., Simeone, P., Trerotola, M., De Domenico, S., Fournier, I., et al. (2017). β-catenin knockdown affects mitochondrial biogenesis and lipid metabolism in breast cancer cells. Front. Physiol. *8*, 544.

Vyas, S., Zaganjor, E., and Haigis, M.C. (2016). Mitochondria and cancer. Cell *166*, 555–566.

Wagner, K.W., Alam, H., Dhar, S.S., Giri, U., Li, N., Wei, Y., Giri, D., Cascone, T., Kim, J.H., Ye, Y., et al. (2013). KDM2A promotes lung tumorigenesis by epigenetically enhancing ERK1/2 signaling. J. Clin. Invest. *123*, 5231–5246.

Wen, Y.A., Xiong, X., Scott, T., Li, A.T., Wang, C., Weiss, H.L., Tan, L., Bradford, E., Fan, T.W.M., Chandel, N.S., et al. (2019). The mitochondrial retrograde signaling regulates Wnt signaling to promote tumorigenesis in colon cancer. Cell Death Differ. *26*, 1955–1969.

Whetstine, J.R., Nottke, A., Lan, F., Huarte, M., Smolikov, S., Chen, Z., Spooner, E., Li, E., Zhang, G., Colaiacovo, M., and Shi, Y. (2006). Reversal of histone lysine trimethylation by the JMJD2 family of histone demethylases. Cell *125*, 467–481.

White, E. (2012). Deconvoluting the context-dependent role for autophagy in cancer. Nat. Rev. Cancer *12*, 401–410.

Wilson, A.C., LaMarco, K., Peterson, M.G., and Herr, W. (1993). The VP16 accessory protein HCF is a family of polypeptides processed from a large precursor protein. Cell *74*, 115–125.

Wu, Z., Puigserver, P., Andersson, U., Zhang, C., Adelmant, G., Mootha, V., Troy, A., Cinti, S., Lowell, B., Scarpulla, R.C., and Spiegelman, B.M. (1999). Mechanisms controlling mitochondrial biogenesis and respiration through the thermogenic coactivator PGC-1. Cell *98*, 115–124.

Yang, W., Xia, Y., Ji, H., Zheng, Y., Liang, J., Huang, W., Gao, X., Aldape, K., and Lu, Z. (2011). Nuclear PKM2 regulates β-catenin transactivation upon EGFR activation. Nature *480*, 118–122.

Zhang, H., Gao, P., Fukuda, R., Kumar, G., Krishnamachary, B., Zeller, K.I., Dang, C.V., and Semenza, G.L. (2007). HIF-1 inhibits mitochondrial biogenesis and cellular respiration in VHL-deficient renal cell carcinoma by repression of C-MYC activity. Cancer Cell *11*, 407–420.

Zhang, J., Nuebel, E., Wisidagama, D.R., Setoguchi, K., Hong, J.S., Van Horn, C.M., Imam, S.S., Vergnes, L., Malone, C.S., Koehler, C.M., and Teitell, M.A. (2012). Measuring energy metabolism in cultured cells, including human pluripotent stem cells and differentiated cells. Nat. Protoc. *7*, 1068–1085.

Zong, W.X., Rabinowitz, J.D., and White, E. (2016). Mitochondria and cancer. Mol. Cell *61*, 667–676.

STAR★METHODS

KEY RESOURCES TABLE

REAGENT or RESOURCE	SOURCE	IDENTIFIER
Antibodies		
Rabbit polyclonal antibody anti-PGC-1α K224me	Signalway Biotechnology	N/A
Mouse monoclonal antibody anti-PGC-1α	Millipore	Cat# ST1202; RRID: AB_2043459
Rabbit monoclonal antibody anti-KDM3A	Abcam	Cat# ab191389
Mouse monoclonal antibody anti-MT-CO2	Abcam	Cat# ab79393
Rabbit polyclonal antibody anti-MT-CYB	Abcam	Cat# ab81215; RRID: AB_1860250
Rabbit polyclonal antibody anti-SQSTM1/p62	Abcam	Cat# ab91526; RRID: AB_2050336
Rabbit monoclonal antibody anti-ATG5	Cell Signaling Technology	Cat# 12994; RRID: AB_2630393
Rabbit monoclonal antibody anti-HA	Cell Signaling Technology	Cat# 3724
Rabbit monoclonal antibody anti-LC3B	Cell Signaling Technology	Cat# 3868; RRID: AB_2137707
Rabbit monoclonal antibody anti-NRF1	Cell Signaling Technology	Cat# 46743; RRID: AB_2732888
Rabbit monoclonal antibody anti-PARP	Cell Signaling Technology	Cat# 9532; RRID: AB_659884
Rabbit monoclonal antibody anti-TFAM	Cell Signaling Technology	Cat# 8076; RRID: AB_10949110
Mouse monoclonal antibody anti-α-tubulin	Santa Cruz Biotechnology	Cat# sc-5286; RRID: AB_628411
Mouse monoclonal antibody anti-HIF-1α	BD Biosciences	Cat# 610958; RRID: AB_398271
Rabbit polyclonal antibody anti-HIF-1α	Proteintech	20960-1-AP
Rabbit polyclonal antibody anti-NRF2α/GABPA	ThermoFisher Scientific	Cat# PA5-27735; RRID: AB_2545211
Mouse monoclonal antibody anti-Flag	Sigma-Aldrich	Cat# F3165; RRID: AB_259529
Anti-DYKDDDDK affinity gel	BioLegend	Cat# 651503
Bacterial and Virus Strains		
TOP10	ThermoFisher Scientific	Cat# C404010
Biological Samples		
Human GBM specimens	the First Affiliated Hospital of Nanjing Medical University	N/A
Chemicals, Peptides, and Recombinant Proteins		
chloroquine diphosphate	Sigma-Aldrich	Cat# C6628
DFO	Sigma-Aldrich	Cat# D9533
DAPI	Sigma-Aldrich	Cat# D9542
N-acetyl-L-cysteine	Sigma-Aldrich	Cat# A7250
ascorbate	Sigma-Aldrich	Cat# A4034
α-ketoglutarate	Sigma-Aldrich	Cat# 75892
dimethyl-αKG	Sigma-Aldrich	Cat# 349631
NAD^+	Sigma-Aldrich	Cat# N6522
formaldehyde dehydrogenase	Sigma-Aldrich	Cat# F1879
IOX1	Selleck Chemicals	Cat# S7234
PGC-1α aa214-234 peptides (K224me0)	SynPeptide	N/A
PGC-1α aa214-234 peptides (K224me1)	SynPeptide	N/A
PGC-1α aa214-234 peptides (K224me2)	SynPeptide	N/A
PGC-1α aa214-234 peptides (K224me3)	SynPeptide	N/A
KDM2A recombinant protein	ActiveMotif	Cat# 31485
KDM3A recombinant protein	ActiveMotif	Cat# 31456
KDM4A recombinant protein	ActiveMotif	Cat# 31457
Critical Commercial Assays		
QIAamp DNA mini kit	QIAGENE	Cat# 51304
TRIzol reagent	ThermoFisher Scientific	Cat# 15596026

(*Continued on next page*)

Continued

REAGENT or RESOURCE	SOURCE	IDENTIFIER
iQ SYBR Green Supermix	Bio-Rad	Cat# 170-8882
SimpleChIP plus Enzymatic Chromatin IP kit	Cell Signaling Technology	Cat# 9003
MitoTracker Red CMXRos	ThermoFisher Scientific	Cat# M7512
VECTASTAIN ABC kit	Vector Laboratories	Cat# PK-4000
Liquid DAB+ Substrate Chromogen System	Dako	Cat# K3468
QuikChange site-directed mutagenesis kit	Agilent Technologies	Cat# 200524
DCFDA / H2DCFDA - Cellular ROS Assay Kit	Abcam	Cat# ab113851
DeadEnd Colorimetric TUNEL System	Promega	Cat# G7360
Dual-Luciferase Reporter Assay System	Promega	Cat# E1910
Deposited Data		
Raw Data	This paper, Mendeley Data	https://doi.org/10.17632/wk3myh726s.1
Experimental Models: Cell Lines		
Human: U87	ATCC	Cat# HTB-14
Human: U251	Sigma-Aldrich	Cat# 09063001
Human: T98G	ATCC	Cat# CRL-1690
Human: NHA	Lonza	Cat# CC-2565
Human: MD-MB-231	ATCC	Cat# HTB-26
Human: BxPC-3	ATCC	Cat# CRL-1687
Human: HeLa	ATCC	Cat# CCL-2
Human: HepG2	ATCC	Cat# HB-8065
Human: 293T	ATCC	Cat# CRL-11268
Experimental Models: Organisms/Strains		
Mouse: BALB/c nude	The University of Texas MD Anderson Cancer Center	N/A
Mouse: BALB/c nude	Model Animal Research Center of Nanjing University	N/A
Oligonucleotides		
shRNA sequence targeting PGC-1α: TTACCGACATAAATCACAC	N/A	N/A
shRNA sequence targeting KDM3A #1: TGATCATGAATAGGATCGT	This paper	N/A
shRNA sequence targeting KDM3A #2: TTCCTGAACAGTTATTAGG	This paper	N/A
shRNA sequence targeting HIF-1α: TTCATATCCAGGCTGTGTC	This paper	N/A
Primers used in this paper, see Table S1	This paper	N/A
Recombinant DNA		
Flag-PGC-1α	This paper	N/A
Flag-PGC-1α K224R	This paper	N/A
Flag-rPGC-1α	This paper	N/A
Flag-rPGC-1α K224R	This paper	N/A
Flag-PGC-1α 1-403	This paper	N/A
Flag-PGC-1α 404-798	This paper	N/A
Flag-PGC-1α ΔRRM	This paper	N/A
Flag-PGC-1α ΔSR	This paper	N/A
Flag-KDM3A	This paper	N/A
Flag-KDM3A H1120Y	This paper	N/A
Flag-rKDM3A	This paper	N/A
Flag-rKDM3A H1120Y	This paper	N/A

(*Continued on next page*)

Continued

REAGENT or RESOURCE	SOURCE	IDENTIFIER
HA-KDM3A	This paper	N/A
HA-KDM3A H1120Y	This paper	N/A
Flag-KDM1A	This paper	N/A
Flag-KDM2A	Wagner et al., 2013	N/A
Flag-Kdm2b	He et al., 2013	Addgene# 61739
Flag-KDM4A	This paper	N/A
Flag-KDM4B	This paper	N/A
Flag-KDM4C	This paper	N/A
Flag-Kdm4d	Matoba et al., 2014	Addgene# 61553
Flag-Kdm5b	This paper	N/A
Flag-KDM5C	This paper	N/A
Flag-KDM5D	Li et al., 2016a	N/A
Flag-KDM6A	This paper	N/A
Flag-KDM6B	This paper	N/A
Flag-KDM6C	This paper	N/A
Flag-KDM7A	Osawa et al., 2011	N/A
Flag-KDM7C	This paper	N/A
Flag-KDM8	This paper	N/A
Flag-HR	Liu et al., 2014	N/A
HA-ERRα	This paper	N/A
HA-PPARα	This paper	N/A
HA-YY1	This paper	N/A
HA-NRF1	This paper	N/A
HA-HCF1	Wilson et al., 1993	Addgene# 53309
PX458 (pSpCas9(BB)-2A-GFP)	Ran et al., 2013	Addgene# 48138
pGL3-TFAM/NRF1-Luc	This paper	N/A
pGL3-TFAM/NRF2α-Luc	This paper	N/A
pGL3-TFB1M(−201)-Luc	This paper	N/A
pGL3-TFB2M(−80)-Luc	This paper	N/A
Software and Algorithms		
ImageJ	NIH	N/A
CRISPR Design tool	Zhang Lab	http://zlab.bio/guide-design-resources

LEAD CONTACT AND MATERIALS AVAILABILITY

Further information and requests for resources and reagents should be directed to and will be fulfilled by the Lead Contact, Zhimin Lu (zhiminlu@zju.edu.cn).

EXPERIMENTAL MODEL AND SUBJECT DETAILS

Mice

We intracranially injected 1×10^6 cells suspended in 5 μl of Dulbecco's modified Eagle's medium into 4-week-old female athymic nude mice, as described previously (Yang et al., 2011). Seven mice were included in each group. Mice were fed with autoclaved food and water and maintained in s specific-pathogen-free facility. For hypoxia treatment, mice were raised in a controlled oxygen tension (11%) chamber (GC-A01, Longfujia Life Sciences Ltd., Beijing, China). Mice were sacrificed 28 days after injection. Their brains were harvested, fixed in 4% formaldehyde, and embedded in paraffin. Tumor formation was determined by H&E staining. Tumor volume was calculated by $0.5 \times L^2 \times W$ (L, length; W, width). The use of animals was approved by the Institutional Review Board of Nanjing Medical University (Nanjing, China).

Human subjects and immunohistochemical staining

50 primary GBM specimens were obtained from the First Affiliated Hospital of Nanjing Medical University. Sections of paraffin-embedded human GBM tissues were stained with antibodies against PGC-1α K224 monomethylation, total PGC-1α, or HIF-1α. The staining of the tissues was then quantitatively scored according to the percentage of positive cells and staining intensity as described previously (Qian et al., 2017). The following proportion scores were assigned to the sections: 0 if 0% of tumor cells exhibited positive staining, 1 for 0 to 1% positive cells, 2 for 2% to 10% positive cells, 3 for 11% to 30% positive cells, 4 for 31% to 70% positive cells, and 5 for 71% to 100% positive cells. In addition, the staining intensity was scored on a scale of 0-3: 0, negative; 1, weak; 2, moderate; and 3, strong. The proportion and intensity scores were then added to obtain a total score ranging from 0 to 8 as described previously (Qian et al., 2017). The use of human GBM samples and the clinical parameters were approved by the Institutional Review Board of Nanjing Medical University (Nanjing, China).

Cell culture and hypoxia treatment

U87, U251, T98G, NHA, MDA-MB-231, BxPC-3, HeLa, HepG2, and 293T cells were maintained in Dulbecco's modified Eagle's medium supplemented with 10% fetal bovine serum (Hyclone, Logan, UT). For generating shRNA-depleted stable cell lines, cells were transfected with shRNA plasmids targeting PGC-1α or KDM3A, and selected by puromycin. For generating gene-expressing stable cell lines, shRNA-depleted cells were transfected with lentivirus carrying shRNA-resistant (r) WT rPGC-1α, rPGC-1α K224R, WT rKDM3A, or rKDM3A H1120Y, and selected by hygromycin. For hypoxia treatment, cells were incubated in a Ruskinn InvivO$_2$ workstation and oxygen tension was set to 1% unless otherwise indicated.

METHOD DETAILS

Materials

Rabbit polyclonal antibody against PGC-1α K224 monomethylation (PGC-1α K224me) was produced by Signalway Antibody (College Park, MD). A peptide containing PGC-1α K224 monomethylation was injected into rabbits. The rabbit serum was collected and sequentially purified using an affinity column conjugated with non-methylated, demethylated, and trimethylated PGC-1α K224 peptide, respectively, to exclude the antibodies recognizing non-K224-monomethylated PGC-1α, followed by an affinity column conjugated with monomethylated PGC-1α K224 peptide to bind to and purify the PGC-1α K224me antibody. The antibody was then eluted and concentrated. The antibody against PGC-1α (ST1202) was from Millipore (Burlington, MA). Antibodies against MT-CO2 (ab79393), MT-CYB (ab81215), p62 (ab91526), and KDM3A (ab191389) were purchased from Abcam (Cambridge, UK). Antibodies against LC3B (#3868), ATG5 (#12994), HA (#3724), NRF1 (#46743), TFAM (#8076), and PARP (#9532) and the ChIP assay kit were from Cell Signaling Technology (Danvers, MA). Antibodies against α-tubulin (sc-5286), normal rabbit IgG, and normal mouse IgG were from Santa Cruz Biotechnology (Santa Cruz, CA). The antibodies against HIF-1α were from BD Biosciences (610958, San Jose, CA) and Proteintech (20960-1-AP, Rosemont, IL), respectively. The antibody against NRF2α (PA5-27735), as well as anti-HA magnetic beads and mitoTracker Red CMXRos, were from ThermoFisher Scientific (Waltham, MA). Mouse monoclonal antibody against Flag, chloroquine diphosphate, DFO, DAPI, N-acetyl-L-cysteine, ascorbate, $Fe(NH_4)_2(SO_4)_2$, α-ketoglutarate (αKG), dimethyl-αKG, and formaldehyde dehydrogenase were from Sigma-Aldrich (St. Louis, MO). Active KDM2A, KDM3A, and KDM4A recombinant proteins were purchased from ActiveMotif (Carlsbad, CA). Anti-DYKDDDDK (Flag) tag affinity gel was purchased from BioLegend (San Diego, CA). IOX1 was purchased from Selleck Chemicals (Houston, TX). PGC-1α aa214-234 peptides containing K224me0, K224me1, K224me2, or K224me3 were synthesized by SynPeptide (Shanghai, China).

DNA construction and mutagenesis

Polymerase chain reaction (PCR)-amplified human PGC-1α, KDM3A, NRF1, NRF2α, ERRα, PPARα, and YY1 were cloned into pcDNA3.1/hygro(+)-Flag or pcDNA3-HA vector. PGC-1α K224R and KDM3A H1120Y were generated using the QuikChange site-directed mutagenesis kit (Stratagene, La Jolla, CA). shRNA-resistant (r) PGC-1α or KDM3A was made by introducing non-sense mutations in shRNA-targeting sites, as described previously (Qian et al., 2017). pGIPZ vectors carrying shRNAs targeting PGC-1α, HIF-1α, and KDM3A were purchased from Dharmacon (Lafayette, CO). cDNAs of KDM1A, KDM2A (Wagner et al., 2013), Kdm2b (He et al., 2013), KDM4A, KDM4B, KDM4C, Kdm4d (Matoba et al., 2014), Kdm5b, KDM5C, KDM5D (Li et al., 2016a), KDM6A (Wilson et al., 1993), KDM6B, KDM6C, KDM7A (Osawa et al., 2011), KDM7C, KDM8, HR (Liu et al., 2014), NRF1, YY1, and HCF1 (Wilson et al., 1993) were requested from previous reports or from Dharmacon and cloned into pcDNA3.1/hygro(+)-Flag vector. Luciferase reporters were constructed by inserting promoter regions of *TFAM*, *TFB1M*, and *TFB2M* into pGL3-basic vector (Promega, Madison, WI). The primers used for reporter cloning are listed in Table S1.

Transfection

For plasmid transfection, cells were plated at a density of 4×10^5 per 60-mm dish or 1×10^5 per well of a 6-well plate 18 h before transfection. The transfection procedure was performed as previously described (Qian et al., 2018).

CRISPR/Cas9-mediated genomic editing

Genomic mutations were introduced into cells using a CRISPR/Cas9 system as described previously (Ran et al., 2013). Single-guided RNAs (sgRNAs) were designed using the CRISPR design tool (http://zlab.bio/guide-design-resources). The annealed guide RNA oligonucleotides were inserted into PX458 vector (Addgene, Cambridge, MA) digested with the *Bbs*I restriction enzyme. Cells were seeded at 60% confluence overnight, followed by co-transfection of sgRNAs (0.5 μg) with a single-stranded donor oligonucleotide (ssOND, 10 pmol) as a temple to introduce mutations, or without ssOND to introduce indel mutations. Twenty-four hours after transfection, GFP-positive cells were sorted and seeded into 96-well plates. After 3-4 weeks of culture, genomic DNA was extracted from each colony, followed by sequencing of the sgRNA target regions. The primers used for sgRNA cloning and genomic DNA sequencing are listed in Table S1.

Measurement of mitochondrial DNA content

Total DNA was extracted with the QIAamp DNA mini kit (QIAGENE, Germantown, MD) according to the manufacturer's instructions. Mitochondrial DNA content was measured by qRT-PCR of total DNA by assessing the relative levels of mitochondrial DNA D-Loop structure and mitochondrial DNA-encoded *MT-CO*$_2$ versus genomic DNA-encoded *β-actin*. The primers used are listed in Table S1.

Assessment of mitochondrial content

Mitochondria were labeled by incubating cells with media containing 0.2 μM MitoTracker Red CMXRos (Invitrogen) for 25 min at 37°C. Cells were then washed and analyzed by flow cytometry.

Measurement of intracellular ROS

Intracellular ROS was measured by the fluorescence probe DCFDA (Abcam) following the manufacturer's instructions. In brief, 2×10^4 cells were seeded in a clear-bottom 96-well plate. HBSS was pre-equilibrated to hypoxia before using. After treatment with or without hypoxia, cells were washed with HBSS, followed by incubation with 25 μM DCFDA-containing HBSS for 30 min at 37°C in the dark. Green fluorescence was measured with a Synergy HT microplate reader (BioTek) at 485/535 nm.

Apoptosis analysis

Apoptotic cells were analyzed by using DAPI staining as described before (Jeon et al., 2012). Cells (1×10^5) were seeded in a 6-well plate overnight. Cells were then fixed by direct addition of formaldehyde (final concentration 12%) to the culture medium. After fixation, the cells were stained with DAPI (1 μg/ml) for 5 min, followed by washing with PBS. Cells with condensed and/or fragmented chromatin were indicative of apoptosis and counted. For the TUNEL assay, mouse tumor tissues were sectioned at 5-μm thickness. Apoptotic cells were counted using the DeadEnd Colorimetric TUNEL System (Promega) according to the manufacturer's instructions.

Cell viability analyses

A total of 2×10^5 cells was seeded and cultured with or without hypoxia treatment. The viable cells were stained with trypan blue (0.5%) and counted using a Beckman Coulter cell counter.

Cell proliferation analyses

A total of 4×10^4 cells was seeded in 6-well plates. The cells in each well were trypsinized and counted on the indicated days after seeding.

Immunoprecipitation and immunoblotting assay

The extraction of proteins using a modified buffer (50 mM Tris-HCl [pH 7.5], 0.01% of SDS, 1% of Triton X-100, 150 mM NaCl, 1 mM dithiothreitol, 0.5 mM EDTA, 100 μM PMSF, 100 μM leupeptin, 1 μM aprotinin, 100 μM sodium orthovanadate, 100 μM sodium pyrophosphate, and 1 mM sodium fluoride) from cultured cells was followed by immunoprecipitation and immunoblotting analyses using corresponding antibodies, as described previously (Lu et al., 1998). Briefly, for immunoprecipitation, 1 mg protein lysates were incubated with 10 μg antibodies. After overnight incubation at 4°C, protein G-agarose beads were added and left for 3 h. The beads were then washed by the lysis buffer for 4 times. Immunocomplexes were analyzed by immunoblotting assay with indicated antibodies.

Immunofluorescent analyses

Cells were fixed and incubated with the primary antibodies at a dilution of 1:100, fluorescence dye-conjugated secondary antibodies, and DAPI according to standard protocols. The cells were examined by a deconvolutional microscope (Zeiss). The AxioVision 4 software program (Zeiss) was used to deconvolve Z series images. The immunofluorescent intensity was calculated by ImageJ.

Mass spectrometry

Immunoprecipitated Flag-PGC-1α protein from hypoxia-treated U87 cells was digested and analyzed by liquid chromatography-tandem mass spectrometry/mass spectrometry on an Orbitrap-Elite mass spectrometer (ThermoFisher Scientific) to identify post-translational modifications of PGC-1α, as described previously (Qian et al., 2017).

qRT-PCR

RNA was purified using TRIzol reagent (ThermoFisher Scientific) and reverse transcribed using iScript Reverse Transcription Supermix for RT-qPCR (Bio-Rad) according to the manufacturers' instructions. qRT-PCR analyses were performed on a CFX96 Real-Time PCR Detection System (Bio-Rad). The primers used are listed in Table S1.

In vitro demethylation assay

To prepare purified KDM3A and KDM3A H1120Y demethylases, we transfected WT Flag-KDM3A or Flag-KDM3A H1120Y mutant into 293T cells. Cells were lysed with lysis buffer containing 50 mM Tris (pH 7.5), 150 mM NaCl, 1% of NP40, and 0.5 mM EDTA. Demethylases were immunoprecipitated with anti-DYKDDDDK (Flag) tag affinity gel (BioLegend), washed with lysis buffer five times and EDTA-free lysis buffer three times, and eluted with 400 mg/ml of Flag peptide (Sigma-Aldrich). For the demethylase reaction, 200 ng of proteins were incubated in 100 μL of demethylase reaction buffer containing 20 mM Tris-HCl (pH 7.5), 150 mM KCl, 50 μM $Fe(NH_4)_2(SO_4)_2$, 1 mM α-ketoglutarate, and 1 mM ascorbate for 2 h at 37°C, as described previously (Whetstine et al., 2006). Reactions were terminated by boiling for 5 min in SDS sample loading buffer and analyzed by immunoblotting.

Measurement of oxygen consumption rate (OCR)

The extracellular oxygen consumption was determined by OCRs using the Seahorse XF24 extracellular flux analyzer (Seahorse Bioscience) as described before (Li et al., 2016b). 3×10^4 cells were seeded 24 h before the assay. Baseline mitochondrial respiration were recorded at different time points. Compounds including oligomycin, FCCP, antimycin A, and rotenone were sequentially injected to measure oxygen consumption for ATP production, proton leak, maximal respiration, spare respiration, and non-mitochondrial respiration according to the manufacturer's instructions. Hansatech oxygen electrode was used to measure the total cellular oxygen consumption under hypoxia according to the manufacturer's instructions and previous report (Zhang et al., 2012).

Km determination

The *K*m of KDM3A demethylating PGC-1α K224 monomethylation under various oxygen tensions was determined by demethylation-formaldehyde dehydrogenase-coupled reaction assay, as described previously (Shi et al., 2004). The demethylation reaction was performed at 1%, 2.5%, 5%, 7.5%, 10%, 15%, and 21% oxygen at 37°C using an $InvivO_2$ Hypoxic Workstation (Ruskinn Technology). All assay components were pre-equilibrated at the desired oxygen tension for 30 min. Reactions were performed by mixing 0.5 μg recombinant active KDM3A (ActiveMotif, Carlsbad, CA) and 100 μM K224-monomethylated PGC-1α peptide (214-LTTNDDPPHTKme1PTENRNSSRD-234) in 25 μL reaction buffer (20 mM Tris-HCl [pH 7.5], 150 mM KCl, 50 μM $Fe(NH_4)_2(SO_4)_2$, 1 mM α-ketoglutarate, and 1 mM ascorbate). After incubation for 10 min, the reactions were terminated with 250 μM DFO. Twenty microliters of the resulting demethylation reaction were added into 100 μL buffer containing 50 mM potassium phosphate (pH 7.2), 2 mM NAD^+, and 0.1 U of formaldehyde dehydrogenase (Sigma-Aldrich) and incubated for 10 min at 37°C. Values of OD_{340} were measured. Standard curves were obtained from various concentrations of formaldehyde (36%, EMD). *K*m was estimated using Lineweaver-Burk transformation of the Michaelis-Menten kinetic equation.

Luciferase assay

The co-transcriptional activities of PGC-1α were measured as previously described (Fang et al., 2007). 1×10^4 U87 cells were seeded in 24-well plates overnight. Luciferase reporter (0.2 μg) and *Renilla* control plasmid (0.05 μg) were co-transfected overnight, followed by culturing in hypoxia for 24 h. Luciferase activities were measured using the Dual-Luciferase Reporter Assay System (Promega) according to the manufacturer's instructions. Relative levels of luciferase activities were normalized to the levels of *Renilla* control.

ChIP assay

A ChIP assay was performed using a SimpleChIP plus Enzymatic Chromatin IP kit (Cell Signaling Technology). Chromatin prepared from cells in a 10-cm dish was used to determine the total DNA input and was incubated with specific antibodies or normal mouse IgG. The primer sequences used for PCR are listed in Table S1.

Transmission electron microscopy

Cells were fixed with a solution containing 3% of glutaraldehyde plus 2% of paraformaldehyde in 0.1 M cacodylate buffer (pH 7.3) and then washed in 0.1 M sodium cacodylate buffer and treated with 0.1% of Millipore-filtered cacodylate-buffered tannic acid, fixed with 1% of buffered osmium, and stained *en bloc* with 1% Millipore-filtered uranyl acetate. Cells were dehydrated in increasing concentrations of ethanol, infiltrated, and embedded in LX-112 medium. Cells were polymerized in a 60°C oven for approximately 3 days. Ultrathin sections were cut in a Leica Ultracut microtome (Leica, Deerfield, IL), stained with uranyl acetate and lead citrate in a Leica EM Stainer, and examined in a JEM 1010 transmission electron microscope (JEOL, USA, Inc., Peabody, MA) at an accelerating

voltage of 80 kV. Digital images were obtained using the AMT Imaging System (Advanced Microscopy Techniques Corp., Danvers, MA).

QUANTIFICATION AND STATISTICAL ANALYSIS

Statistical analyses were conducted with a two-tailed unpaired Student's t test unless specifically indicated. All data represent the mean ± standard deviation (SD) of three independent experiments/samples unless otherwise specified. Differences in means were considered statistically significant at $p < 0.05$. Significance levels are: *$p < 0.05$; **$p < 0.001$; n.s., no significance. Analyses were performed using the Microsoft Excel.

DATA AND CODE AVAILABILITY

Raw data have been deposited to Mendeley Data and are available at https://doi.org/10.17632/wk3myh726s.1.